ASTRONOMY & ASTROPHYSICS
SUPPLEMENT SERIES

Astron. Astrophys. Suppl. Ser. **119,** 7-24 (1996)

New weak-line T Tauri stars in Orion from the ROSAT all-sky survey⋆

J.M. Alcalá[1,7], L. Terranegra[2], R. Wichmann[3], C. Chavarría-K.[4], J. Krautter[3], J.H.M.M. Schmitt[1], M.A. Moreno-Corral[5], E. de Lara[5] and R.M. Wagner[6]

[1] Max-Planck-Institut für Extraterrestrische Physik, D-85740 Garching, Germany
[2] Osservatorio Astronomico di Capodimonte, Via Moiariello 16, I-80131 Napoli, Italy
[3] Landessternwarte-Königstuhl, D-69117 Heidelberg, Germany
[4] Max-Planck-Institut für Astronomie Königstuhl, D-69117 Heidelberg , Germany
[5] Instituto de Astronomía, Ensenada B.C., México CP 22860
[6] Lowell Observatory, 1400 West Mars Hill Road. Flagstaff, Az 86001, U.S.A.
[7] Instituto Nacional de Astrofísica Optica y Electrónica, A.P. 51 y 216 C.P. 72000, Puebla, México

Received September 20, 1995; accepted January 26, 1996

Abstract. — We present results of the spectroscopic and photometric follow-up observations of the *ROSAT* all-sky survey in the direction of the Orion cloud complex. The main goal of these observations is the search for X-ray emitting pre-main sequence stars. 820 X-ray sources were detected with high confidence in about 450 square degrees. The mean density of X-ray sources in this region is a factor of about two higher than that of the whole RASS. 5% of the RASS sources in this region are identified with previously known and likely pre-main sequence stars. We have investigated spectroscopically 181 new RASS sources widely distributed over the entire cloud complex. On the basis of the presence of strong Li I λ6707 absorption, spectral type later than F0 and chromospheric emission, 112 new weak-line T Tauri stars could be found. We present coordinates, X-ray count-rates and finding charts of the new PMS. Optical $UBV(RI)_{\rm KC}$, near-infrared $JHKLM$ and *uvby-β* photometry for the new WTTS is also provided. In addition 24 dKe-dMe stars were also found on the basis of the RASS data.

Key words: X-rays: stars — stars: pre-main-sequence — ISM: Orion star forming region

1. Introduction

From observations carried out with the *EINSTEIN* satellite in star forming regions (SFRs), it is well known that T Tauri stars can be detected in X-rays with luminosities in the range $L_{\rm X} = 10^{29}$–10^{32} erg/s (Feigelson 1987; Ku & Chanan 1979; Walter et al. 1988, and references therein). These observations led to the discovery of a large number of "weak-line" T Tauri stars (WTTS). These low-mass ($M \leq 3\ M_{\odot}$) pre-main sequence (PMS) stars as their classical counterparts, the classical T Tauri stars (CTTS), show strong Li I λ6707 absorption in their optical spectra. Since Li I is rapidly destroyed in the convective layers of low-mass stars in the early phases of the stellar evolution (Bodenheimer 1965), its presence is used as an indicator of extreme youth. While the CTTS can be easily detected by their strong Balmer emission lines in objective-prism surveys or through their IR excesses, WTTS lack both characteristics. This has been ascribed to the absence of dense circumstellar matter in WTTS. Thus, WTTS are more easily detected on the basis of their X-ray emission.

Before the survey carried out by the X-ray satellite *ROSAT* (Röntgensatellit), all X-ray observations in SFRs were strongly concentrated towards specific areas containing CTTS, and no information about the spatial distribution of X-ray sources far from molecular clouds was available. The *ROSAT* all-sky survey (RASS) provides a spatially unbiased sample of X-ray sources at about the same sensitivity of *EINSTEIN* pointed mode observations thus offering the possibility to carry out an extensive study of the spatial distribution of X-ray emitting PMS stars by using a spatially complete sample of X-ray sources.
With the aim to identify the RASS X-ray sources in SFRs, a long-term project was started (Krautter et al. 1994). The

Send offprint requests to: J.M. Alcalá
⋆Partially based on observations collected at the German Spanish Astronomical Center in Calar Alto, Spain, at Observatory of the Ohio State University in Flagstaff, Arizona, U.S.A. and at the San Pedro Mártir Observatory, UNAM, México

main purpose of this program is the search for WTTS in nearby (closer than 500 pc) SFRs.

The Orion cloud complex at a distance of about 460 pc (Genzel & Stutzki 1989), is a suitable region to study the star formation process, the content of the young stellar population and the interaction of the stellar members with their environment. X-rays observations in Orion have been carried out for the first time by the *Uhuru* satellite (Giacconi & Gursky 1974) and by the *EINSTEIN* satellite (Gagné & Caillault 1994, and references therein). However, all these observations have been restricted to regions in or near the Orion nebula, with no information about the possible presence of X-ray emitting PMS stars far from the cloud complex.

In this paper we report the observations of the RASS in the direction of the Orion SFR and focus on the optical identification of the detected X-ray sources. We give coordinates, X-ray count rates and finding charts of the X-ray sources identified spectroscopically as new WTTS. We also provide $UBV(RI)_{\rm KC}$, $JHKLM$ and *uvby*-β photometry for a sub-sample of the new WTTS. In a forthcoming paper we analyse the optical counterparts identified as low-mass PMS stars, in particular, relationships between their location in the cloud and the main stellar parameters, and of the latter with X-ray properties of the studied stars.

We stress that very large samples of X-ray sources, like the RASS sample in Orion, require several years of identification work. Excluding the sources previously known from *EINSTEIN* observations in this SFR, the sample of RASS sources identified in our spectroscopic study is complete to about 20% by now. Since the RASS is flux limited and because of the large distance of the Orion SFR, this sample may be biased towards the brightest X-ray sources. Although we knew in advance that such a program of spectroscopic identifications would require several years to be completed, we think it is very important to publish the sample of new WTTS. Such a sample is very suitable for future studies of PMS stellar activity and its connection with the evolution of angular momentum in the early phases of the stellar evolution by measuring rotational velocities through high-resolution spectroscopic observations and/or photometric determinations of rotational modulations.

2. The ROSAT all-sky survey in Orion

The telescope, the position-sensitive proportional counter (PSPC) detector and the observing procedure used during the RASS are discussed in detail by Trümper et al. (1991) and Pfeffermann et al. (1986). RASS exposure times depend on the ecliptic latitude β. For the Orion SFR, the exposure times range from 350 s to 800 s.

From previous recent studies of RASS X-ray sources in nearby SFRs, it is known that WTTS occupy a larger area on the sky than the CTTS (Alcalá et al. 1995, henceforth A95; Wichmann et al. 1995, henceforth W95). For our study in Orion, we have selected an area within the (J2000) coordinates: $\alpha_{\rm min} = 5^{\rm h}$, $\alpha_{\rm max} = 6^{\rm h}$, $\delta_{\rm min} = -14^{\circ}$, $\delta_{\rm max} = +16^{\circ}$. This area includes Orion's bright nebula, the molecular clouds A (L1641) and B (L1630) described by Maddalena et al. (1986) and Blaauw (1991). The λ Orionis region located at the north of the Orion OB1 association is also included. Within the selected area, 820 X-ray sources were detected with high confidence using the processing of the Standard Analysis Software System (SASS) (Voges et al. 1992a).
Of particular interest is the density of X-ray sources found in this region. While the mean density of sources for the whole RASS is about 1, there are about 2 sources per square degree in the Orion SFR.

2.1. *Source detection*

The processing of the RASS data was performed using the Extended Scientific Analysis System (EXSAS, Zimmermann et al. 1994) as described in A95 and Neuhäuser et al. (1995). From this processing, the X-ray count rate for each source, the corresponding count errors and the likelihood of the detection are obtained. The typical (2σ) X-ray error circle for most of the sources has a radius not larger than $40''$, which is in good agreement with the determination of Neuhäuser et al. (1995) for RASS sources in the Taurus-Auriga region. All the SASS X-ray sources were recovered in the EXSAS processing. Thus, the identification described below was performed on the 820 X-ray sources detected from both the SASS and the EXSAS processing. For the search of optical counterparts we used a $40''$ radius as a high confidence level error circle.

The spatial distribution of the RASS X-ray sources in the Orion SFR has been discussed by Sterzik et al. (1995). They used 98 of the 112 new WTTS found in the present work (see Sect. 3.2) as the WTTS training sample to preselect potential PMS candidates. In their predicted spatial distribution they find the presence of different concentrations of X-ray emitting PMS stars rather far from the star forming dark clouds.

2.2. *Variable X-ray sources*

Following the procedure described in A95, we obtained X-ray light curves for some 200 RASS sources detected with a count rate greater than 0.08 cts/s. Only the X-ray sources RXJ0534.0-0221, RXJ0530.3-1308 and RXJ0534.6+1007 show significant variations (Fig. 1). The source RXJ0534.6+1007 is identified with a new WTTS (see Sect. 3.2 and Table 3), while the sources RXJ0534.0-0221 and RXJ0530.3-1308 are identified with previously unknown active stars, the former with a dM1e and the latter with a dK2e (see also Sect. 3.2). Other sources may have apparently small scale variability. However, the low signal-to-noise of the RASS data prevent us on carrying

out a finer analysis of the light curves and to determine the nature of this variations. Thus, we cannot exclude the presence of low-level variability observable as scan-to-scan variations.

3. Identification of the X-ray sources

The identification of the X-ray sources consisted of two steps: first, all positional coincidences with objects contained in several astronomical catalogues held in the SIMBAD database and other catalogues (see below) were searched; secondly, the new X-ray sources were investigated by means of mid-resolution spectroscopic observations. Since our main goal in this investigation is the search for X-ray emitting PMS stars, only those sources for which a likely PMS counterpart was found in the present work or elsewhere will be considered hereafter.

3.1. *Identification in catalogues*

In Table 1 we list the coordinates and count rates of the RASS sources in Orion identified with previously known and likely PMS stars. In Col. (8) of this table we list the (broad-band X-ray flux) count rates, while in Col. (10) we give the distance between the X-ray position and it optical counterpart. These identifications were carried out by positional cross correlation with the SIMBAD catalogue, the Herbig & Bell catalogue (1988) and the catalogues Hα line emission objects and/or variables associated with the Orion SFR by Duerr et al. (1982) which is a list of Hα emission line objects found on the basis of an objective-prism survey in the λ Orionis region and the catalogue by Brand & Wouterloot (1990) which compiles a list of about 1385 variable and emission line stars in the Orion SFR. An optical PMS counterpart was associated to a RASS X-ray source when their respective positions were coincident within the 2σ error circle given by *ROSAT*. The source RXJ 0534.7-0524, identified with HBC447, was included in our spectroscopic and photometric observations described below in order to confirm it PMS nature.

Forty-six RASS X-ray sources could be identified with very likely PMS stars. Most of these stars have been discovered on the basis of their strong photometric variability or because of their emission line spectra taken in photographic plates or films with an objective-prism Schmidt camera. Thus, most of their optical counterparts are expected to be CTTS. However, this still represents a rather small fraction (5.6%) of the X-ray emitting PMS population discovered with *ROSAT*, i.e. the WTTS (see Sect. 3.3).

3.2. *Spectroscopic identifications*

The spectroscopic observations were carried out using Boller and Chivens Cassegrain spectrographs coupled with the 1.8 m telescope of the Ohio State University (OSU) at the Lowell Observatory in Flagstaff, Arizona, and with the 2.2 m telescope of the Max-Planck Institut für Astronomie at the Calar Alto (CAO) Observatory in Spain. In Table 2 we give information on the observing runs and the instrumental set-up. The spectral resolution given in Table 2 was estimated from the FWHM of the lines on the comparison spectra.

For the observations we produced finding charts using the HST catalogue database in the form of digitized photographic plates and a program available at the MPE in Garching (Voges 1992a, b). More informations are

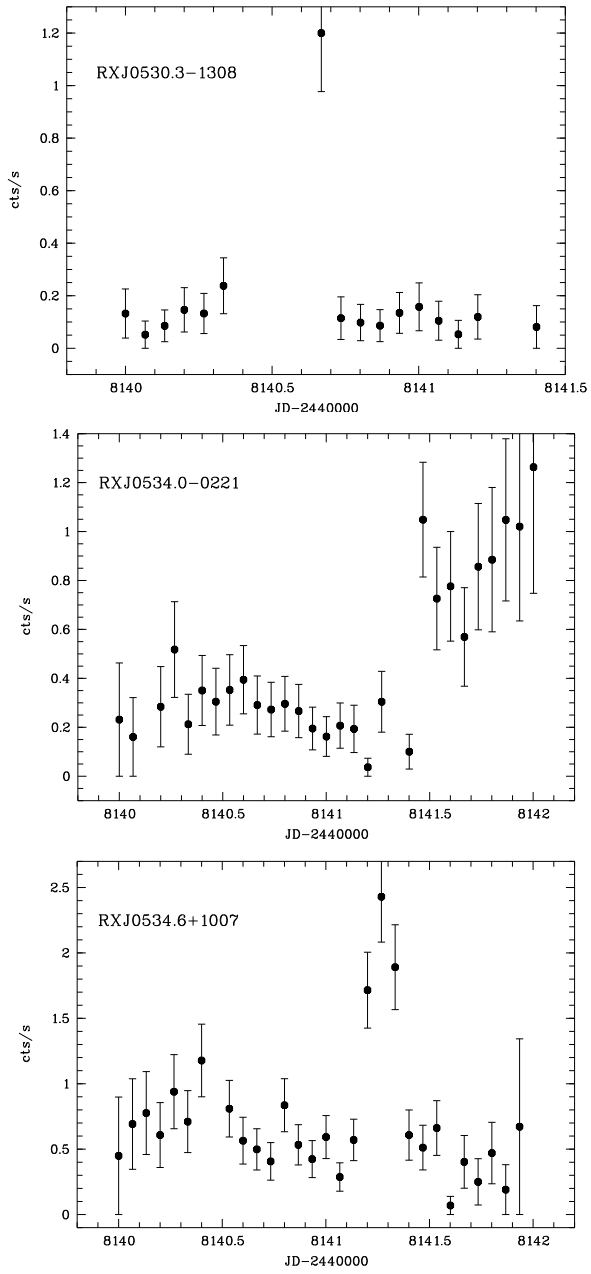

Fig. 1. X-ray light curves of the RASS sources RX 0534.0−0221, RXJ 0530.3−1308 and RXJ 0534.6+1007

Table 1. X-ray sources identified with previously known and likely PMS stars

RXJ	α(2000) h m s	δ(2000) ° ′ ″	cts/s	Ident.	θ [″]	Ref.
0506.2−0408	05 06 12.30	−04 08 17.9	0.06±0.02	AQ ERI	21	1
0512.3−1151	05 12 17.50	−11 51 57.3	1.12±0.06	HD 33802B	5	1
0512.3−0255	05 12 20.00	−02 55 46.3	0.05±0.02	V531 ORI	40	1
0520.5−0548	05 20 29.80	−05 48 14.2	0.04±0.02	EM* STHA 39	21	1
0527.7+1446	05 27 43.30	+14 46 15.3	0.04±0.02	DIL07	10	2
0528.8+1121	05 28 48.20	+11 21 20.6	0.03±0.01	DIL10	10	2
0529.0−0334	05 28 59.90	−03 34 02.0	0.10±0.02	V1159 ORI	16	1
0529.4+1152	05 29 22.00	+11 52 20.4	0.09±0.02	V649 ORI	43	1
0532.6−0522	05 32 36.70	−05 22 50.9	0.12±0.02	HR ORI	27	1
0533.2−0131	05 33 10.90	−01 31 37.7	0.03±0.02	KIHA−4−14	40	3
0533.7−0521	05 33 43.50	−05 21 22.0	0.04±0.02	V730 ORI	23	1
0533.7+0156	05 33 44.80	+01 56 46.1	0.55±0.05	GJ 207.1	8	1
0534.2−0407	05 34 09.10	−04 07 19.0	0.03±0.01	V391 ORI	32	1
0534.6−0606	05 34 38.80	−06 06 29.7	0.05±0.02	V938 ORI	6	1
0534.7−0524	05 34 40.70	−05 24 36.2	0.22±0.03	HBC 447	40	4
0534.8−0534	05 34 45.80	−05 34 17.7	0.07±0.02	V1118 ORI	45	1
0534.9−0542	05 34 51.30	−05 42 21.0	0.11±0.03	V776 ORI	5	1
0535.1−0508	05 35 04.20	−05 08 12.0	0.37±0.04	HBC452	9	4
0535.3−0523	05 35 15.90	−05 23 29.3	2.53±0.10	TRAPEZIUM		
0535.3−0042	05 35 20.30	−00 42 13.9	0.05±0.02	HARO 5−72	5	1
0535.4−0450	05 35 21.40	−04 50 25.5	0.13±0.03	MW ORI	18	1
0535.4−0654	05 35 23.40	−06 54 52.4	0.05±0.02	V796 ORI	40	1
0535.8−0508	05 35 45.00	−05 08 41.2	0.15±0.03	V388 ORI	5	1
0536.0−0616	05 35 59.30	−06 16 16.0	0.09±0.02	V1178 ORI	6	1
0536.0−0650	05 36 00.10	−06 50 09.1	0.05±0.02	WBHA−33	10	3
0536.1−0541	05 36 05.80	−05 41 30.5	0.06±0.02	KIHA−76−114	20	3
0536.1−0509	05 36 08.70	−05 09 45.5	0.08±0.02	V655 ORI	57	1
0536.2−0522	05 36 10.30	−05 22 08.2	0.06±0.02	V391 ORI	27	1
0536.4−0627	05 36 23.70	−06 27 01.3	0.05±0.02	V582 ORI	60	1
0537.7−0508	05 37 39.50	−05 08 45.3	0.02±0.01	V1185 ORI	8	1
0538.5−0717	05 38 32.00	−07 17 10.3	0.02±0.01	KIHA−76−337	20	3
0539.3+0949	05 39 15.70	+09 49 56.8	0.04±0.01	DIL 60	15	2
0539.5−0248	05 39 31.20	−02 48 53.1	0.03±0.01	V957 ORI	60	1
0540.0−0222	05 39 58.80	−02 22 44.0	0.08±0.02	KIHA4−95	20	3
0540.1−0627	05 40 05.50	−06 27 49.5	0.01±0.02	V897 ORI	22	1
0540.7−0211	05 40 44.70	−02 11 47.3	0.22±0.03	KIHA−4−110	10	3
0542.2+1138	05 42 13.80	+11 38 36.6	0.03±0.01	KIHA−4−133	20	3
0542.6+0850	05 42 37.30	+08 50 50.7	0.03±0.01	DIL 74	25	2
0542.9−0718	05 42 56.10	−07 18 46.7	0.12±0.02	V909 ORI	35	1
0543.0+0910	05 43 00.10	+09 10 23.1	0.07±0.02	DIL 75	10	2
0543.0−0218	05 43 00.40	−02 18 46.6	0.12±0.02	EM* LKHA 291	21	1
0543.5+0909	05 43 32.30	+09 09 27.8	0.04±0.01	DIL 78	24	2
0544.6−0121	05 44 34.00	−01 21 55.9	0.05±0.01	V523 ORI	60	1
0547.3−0000	05 47 17.80	−00 00 45.7	0.20±0.03	EM* LKHA 312	60	1
0547.8+0833	05 47 48.50	+08 33 15.4	0.03±0.01	DIL 92	18	2
0552.1−0525	05 52 08.50	−05 25 11.2	0.03±0.01	CN ORI	25	1

(1) Simbad catalogue ; (2) Duerr et al. (1982); (3) Brand & Wouterloot (1990); (4) Herbig & Bell (1988).

Table 2. Journal of spectroscopic observations

Tel.	Period	CCD	Disp. [Å/mm]	Range [Å]	Res. [Å]	No. of Sources investigated	No. of new WTTS
OSU1.8m	20.12.91 - 27.12.91	TI 4849	150	4500–7000	11.5	65	38
CAO2.2m	28.12.91 - 02.01.92	RCA#11	72	5500–6800	3.9	24	18
CAO2.2m	22.12.92 - 29.12.92	TEK#6	72	5500–6800	4.0	29	16
OSU1.8m	02.12.93 - 09.12.93	TEK	72	5500–6800	5.0	28	21
CAO2.2m	16.12.93 - 26.12.93	TEK#6	72	5500–6800	3.7	35	19

obtained from the output of this program apart of the finding chart itself. Namely, the X-ray error circle is drawn and a list of coordinates and photographic magnitudes, $B_{\rm ph}$, of different types of objects (with the specification if star, galaxy or faint), sorted by increasing distance from the X-ray source position, is provided.

In order to avoid any bias in the spatial distribution, we divided the studied area in 12 regions (6 in the coordinate range $5^{\rm h} \leq \alpha \leq 5^{\rm h}$:$30^{\rm m}$ with δ running form $-14°$ to $+16°$ in intervals of $5°$, and the other 6 regions in the coordinate range $5^{\rm H} : 30^{\rm m} \leq \alpha \leq 6^{\rm h}$ with δ running in the same way). The number of investigated X-ray sources is approximately the same ($\approx 15 \pm 1$) in each region. Thus,

the sample of X-ray sources investigated spectroscopically is spatially unbiased.

For each field observational priority was assigned mainly on the basis of the brightness of the objects and their relative position to the error circle: highest priority was given to stars inside the error circle and brighter than about $B_{\rm ph}$=17. From *Einstein* observations in SFRs and from the f_x/f_v ratio for known T Tauri stars, it is expected that X-ray emitting T Tauri stars have V magnitudes in the range 10−16. Furthermore, the T Tauri stars identified in catalogues (Sect. 3.1) are normally brighter than V=15. Since typical $B-V$ colours of T Tauri stars are in the range of 0.3−1.6, we adopted $B_{\rm ph}$=17 as a reasonable limiting magnitude in the search for WTTS (which was also the limiting magnitude of our set-up to get a good sinal-to-noise ratio in reasonable exposure times). If no star brighter than about $B_{\rm ph}$=17 was inside the error circle, the stellar object nearest to the X-ray PSPC position (within a radius of about 60″) and brighter than about $B_{\rm ph}$=17 was observed. Sometimes more than one star brighter than $B_{\rm ph}$=17 was found inside the error circle. In such cases, all these stars were observed.

Typically, 2–3 candidates were observed in each X-ray error circle. The exposure times for the spectroscopic observations were in the range 10−15 minutes for the brightest stars ($V\leq$ 13$^{\rm m}$), and up to 20−35 minutes for the faintest ones ($V\leq$ 16$^{\rm m}$). With these exposure times, a $S/N \approx 70$ was achieved in the best cases. For the wavelength calibration of the stellar spectra, a He-Ar lamp was used to obtain comparison spectra immediately after each object exposure. For flux calibration purposes, 2 to 3 standard stars per night were also observed nightly.
In order to carry out the spectral type classification, a grid of bright ($3^{\rm m} \leq V \leq 6^{\rm m}$) standard stars with very well determined spectral types was observed using the same instrumental set-up.

All the spectra were reduced following the standard procedure of MIDAS software package. A relative flux calibration of each spectrum was performed using a mean response function for each observational run. Since most of the nights were not photometric, only a relative flux calibration of the spectra could be performed.

To classify a star as a WTTS we adopted the same criteria as in A95, namely: presence of the Li I λ6707 absorption line, spectral type later than F0 and eventually the presence of chromospheric Hα emission with equivalent width less than 10 Å. However, the latter is not necessarily a PMS indicator (Walter et al. 1988), since chromospherically active dMe stars show rather strong emission lines like Hα and Ca II H+K, but they are not PMS stars. The K and M stars with Hα in emission but lacking Li I absorption have been classified by us as dKe and dMe stars, respectively.

181 spatially unbiased RASS X-ray sources were investigated spectroscopically in Orion. Of these, 110 were found to be associated with 112 stars showing PMS characteristics (two of these identifications are ambiguous, see below). Other 9 sources are identified with stars showing clear Hα emission or filled-in with emission and marginal evidence of lithium in absorption, but need confirmation because of the low signal-to-noise of their spectra. In addition, 24 sources were found to be associated with previously unknown dKe-dMe stars unrelated to the SFR. Some of these active stars display clear emission at Hα but others show some emission filling-in the line. For the rest of the sources, no stellar counterpart with $V \leq 17^{\rm m}$, i.e. fainter than the limiting magnitude of our spectroscopic observations, could be found. By inspecting the finding charts, we find that the error circles of a major part of these sources contain extragalactic objects and/or faint ($V \geq 18^{\rm m}$) stellar-like objects. Thus, very likely the optical counterparts of these sources are extragalactic objects.

In total, some 438 spectra were obtained. About 60% of the 181 investigated X-ray sources resulted in positive WTTS identifications. This number is fully consistent with the detection rate of RASS discovered WTTS in the Chamaeleon and Taurus-Auriga SFRs (A95, W95). The coordinates and the (broad X-ray flux) count rates of the X-ray sources identified with new WTTS are given in Table 3. In this table, we also include the 9 WTTS candidates for which the presence of lithium absorption has to be confirmed. In Fig. 2 typical spectra of the new WTTS in Orion are shown.

A few sources have ambiguous optical identification, since more than one new PMS star is found in the same error circle. Two sources (RXJ0532.4+0131 and RXJ0538.4-0637) have two WTTS in the same error circle. Also, a WTTS and a dKe star were fount to be associated to the source RXJ0532.4-0713 and two sources (RXJ0500.9+0222 and RXJ0549.7-1158) have two dKe-dMe stars in the same error circle.

The total number of CTTS and WTTS in Orion is still very uncertain. The spectroscopic identification of the RASS sources is far from being complete, and there are many emission line objects in this region for which the PMS nature is not yet confirmed. However, already the RASS WTTS in Orion outnumber the stars in Table 1 by a factor of about 2.5.

3.3. *Spectral types and equivalent widths*

Spectral types were determined by comparison with a grid of bright spectral standard stars (from F0 to M5) observed with the same dispersion and the same instrumental set-up in each observing run, using the same procedure as described in A95. The accuracy of the spectral types is estimated to be about ±1 sub-class in most cases. The spectral types of the WTTS are listed in Table 3.

The equivalent widths of the Hα and Li I lines were obtained using the same procedure as described in A95. The mean standard deviations resulting from several

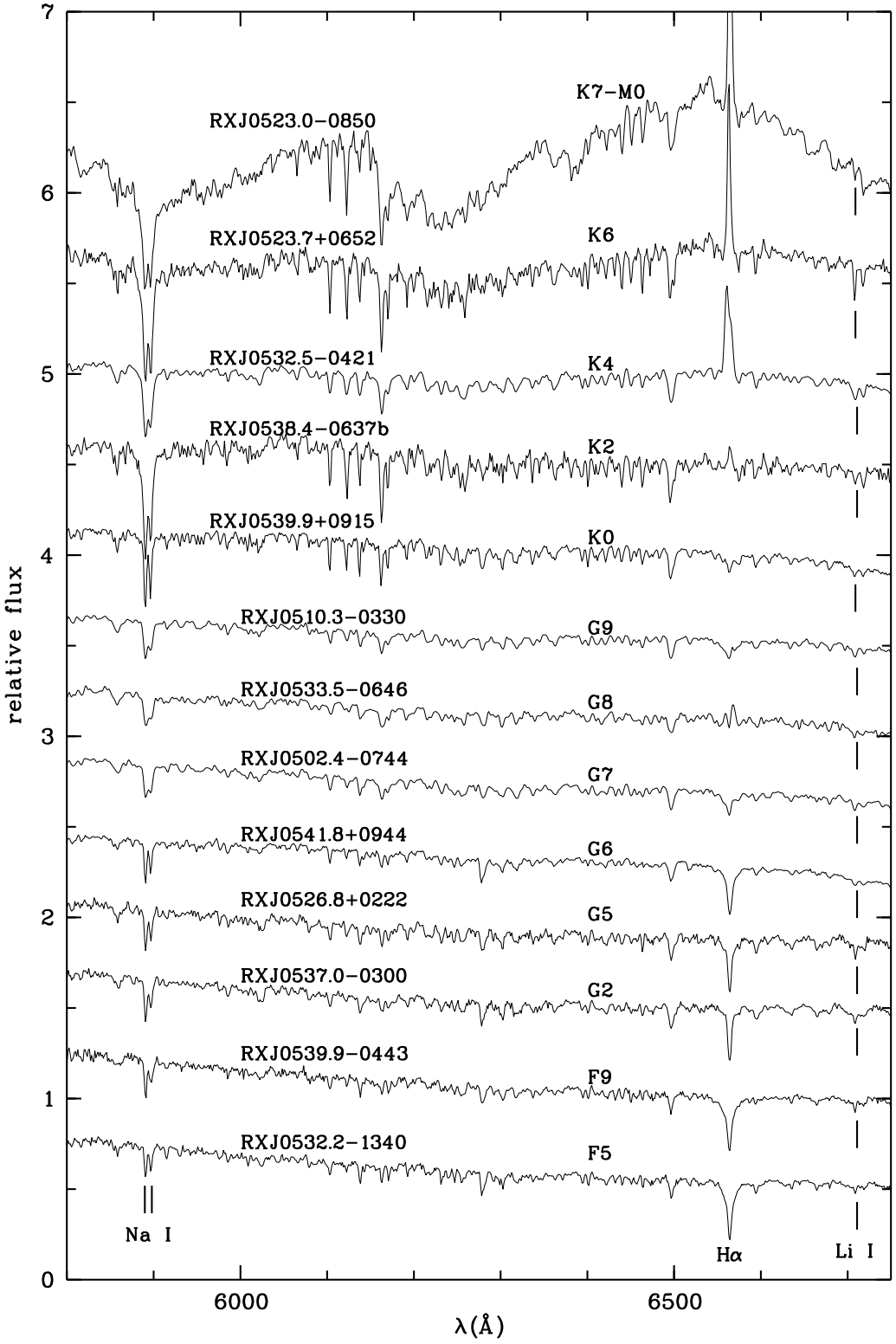

Fig. 2. Examples of typical WTTS spectra in Orion. Each spectrum is normalized to the continuum at $\lambda = 6000$ Å and arbitrary shifted for the sake of comparison

Table 3. RASS sources identified with new WTTS in Orion

RXJ	α(2000) h m s	δ(2000) ° ′ ″	Sp.T.	W(Hα) [Å]	W(Li) [Å]	cts/s
(1)	(2)	(3)	(4)	(5)	(6)	(7)
0500.4−1054	05 00 26.7	−10 54 47.9	K6	−1.80	0.30	0.049±0.018
0501.1+0642	05 01 05.8	+06 42 03.0	K5	−0.55	0.42	0.043±0.013
0502.4−0744	05 02 21.1	−07 44 02.9	G7	+1.70	0.30	0.050±0.015
0503.8−1130	05 03 49.5	−11 30 59.0	K3	+1.50	0.45	0.057±0.016
0506.2+0439	05 06 13.2	+04 39 47.4	M3	−6.50	0.27	0.189±0.028
0507.5+1010	05 07 31.2	+10 10 47.6	K2	+2.30	0.40	0.103±0.026
0507.8−0931	05 07 48.0	−09 31 44.3	K2	+0.80	0.42	0.045±0.015
0509.0−0315	05 08 59.5	−03 15 10.3	K1	+1.80	0.33	0.060±0.016
0510.1−0427	05 10 04.8	−04 27 54.2	K4	−0.20	0.25	0.137±0.031
0510.3−0330	05 10 15.9	−03 30 00.4	G9	+1.40	0.36	0.059±0.023
0511.7−0348	05 11 39.5	−03 48 49.8	K3	+1.85	0.38	0.029±0.017
0512.3−0255	05 12 20.0	−02 55 46.3	K3	−6.70	0.45	0.045±0.016
0513.1+0851	05 13 05.9	+08 51 19.6	K3	−19.50	0.25	0.037±0.015
0513.4−1244	05 13 22.0	−12 44 50.4	G6	+3.00	0.30	0.112±0.029
0515.6−0930	05 15 36.3	−09 30 49.5	G5	+2.50	0.25	0.207±0.036
0517.9−0708	05 17 54.9	−07 08 24.4	K3	+2.10	0.35	0.071±0.025
0518.0−1146	05 17 57.2	−11 46 07.8	K3	−0.01	0.40	0.084±0.023
0518.0+0712	05 18 01.5	+07 12 28.0	K3	+0.30	0.57	0.034±0.016
0518.3+0829	05 18 20.0	+08 29 18.0	G9	+1.50	0.45	0.065±0.019
0518.6+0959	05 18 37.8	+09 59 48.9	K2	+1.70	0.45	0.023±0.012
0519.9+0552	05 19 51.1	+05 52 10.7	K6	−1.25	0.58	0.059±0.019
0520.0+0612	05 20 00.3	+06 12 57.0	K3	−0.20	0.60	0.085±0.023
0520.5+0616	05 20 32.4	+06 16 12.9	K3	−0.90	0.50	0.123±0.028
0520.9−0452	05 20 55.9	−04 52 42.4	F5	+5.00	0.22	0.028±0.014
0522.1−0844	05 22 03.3	−08 44 18.5	K1	+1.45	0.40	0.035±0.015
0522.7+0014†	05 22 43.8	+00 14 32.2	M2	−4.85	–	0.078±0.024
0522.8−1144†	05 22 47.6	−11 44 34.9	M1	−4.90	–	0.027±0.012
0522.9+0857	05 22 54.8	+08 57 50.5	K1	−1.05	0.20	0.261±0.042
0523.0−0850	05 22 57.5	−08 50 20.1	K7-M0	−5.43	0.37	0.072±0.021
0523.1−0440	05 23 03.2	−04 40 36.7	K5	−11.60	0.50	0.026±0.016
0523.7+0652	05 23 42.6	+06 52 01.2	K6	−4.40	0.60	0.055±0.021
0524.1+0730	05 24 06.4	+07 30 56.0	K4	−0.30	0.50	0.026±0.014
0525.3+0208	05 25 15.8	+02 08 56.0	M4	−10.00	0.45	0.056±0.019
0526.5+1510	05 26 32.5	+15 10 02.4	G5	+3.86	0.20	0.019±0.010
0526.7+0143	05 26 42.9	+01 43 48.7	K0	+0.20	0.50	0.041±0.016
0526.8+0222	05 26 47.8	+02 22 02.4	G5	+2.80	0.27	0.070±0.020
0527.7+0153†	05 27 41.3	+01 53 30.3	K7	−1.45	–	0.032±0.015
0528.0−0053	05 27 59.3	−00 53 19.3	K0	+0.25	0.30	0.028±0.014
0528.3+0326	05 28 16.7	+03 26 39.1	K0	+0.50	0.40	0.044±0.016
0528.8+0048	05 28 47.3	+00 48 31.4	K0	+0.40	0.28	0.032±0.014
0528.8+0105	05 28 46.8	+01 05 39.6	K4	+0.30	0.35	0.050±0.015
0529.2−0615	05 29 13.7	−06 15 04.9	K1	+1.10	0.20	0.049±0.018
0529.4+0041	05 29 22.5	+00 41 09.1	K2	−0.01	–	0.048±0.017
0530.1+0041	05 30 05.3	+00 41 18.3	G2	+2.80	0.30	0.193±0.030
0530.7−0434	05 30 43.3	−04 34 59.3	K3	−0.04	0.53	0.050±0.018
0530.9+1015	05 30 55.5	+10 15 05.6	K3	+0.80	0.52	0.067±0.019
0531.2+0118	05 31 09.6	+01 18 52.3	K0	+0.45	0.38	0.022±0.012
0531.6−0326	05 31 38.6	−03 26 55.9	K0	+1.50	0.20	0.083±0.030
0532.1−0732	05 32 05.8	−07 32 43.9	K4	−0.01	0.31	0.050±0.015
0532.2−1340	05 32 14.5	−13 40 58.3	F5	+4.10	0.20	0.082±0.023

measurements of the equivalent widths are: $\sigma = 0.25$ Å for Hα and $\sigma = 0.15$ Å for the Li I line. For late type stars (K and M stars) and for stars with a low S/N ratio, the uncertainty comes mainly from the fit to the continuum. The equivalent width was also measured for the stars with Hα in absorption. These stars have Hα absorption weaker than normal stars of the same spectral type. The equivalent widths are listed in Table 3. In this table, a negative equivalent width means an emission line.

The source RXJ 0534.7-0524 is identified with the star HBC447 (see Table 1). Since its PMS nature was dubious, we decided to include this star in our spectroscopic and photometric observations. The spectrum of the star shows a double-lined peak at Hα and strong Li I λ 6707 Å absorption. We classified the star as a new WTTS. The spectral type we derived is in very good agreement with that given by Herbig & Bell (1988).

3.4. *CTTS candidates ?*

The dividing line between WTTS and CTTS is somewhat controversial. A parameter used to classify low-mass PMS stars as WTTS or CTTS is the equivalent width of the Hα emission line. The limiting value of W(Hα)=−10 Å has been generally adopted (negative equivalent widths indicate emission lines in our convention). Nevertheless, this criterion is purely empirical and may lead to

Table 3. continued

RXJ	α(2000) h m s	δ(2000) ° ′ ″	Sp.T.	W(Hα) [Å]	W(Li) [Å]	cts/s
(1)	(2)	(3)	(4)	(5)	(6)	(7)
0532.4+0131a	05 32 22.6	+01 31 41.6	K2	+1.50	0.40	0.025±0.013
0532.4+0131b	05 32 22.6	+01 31 41.6	K5	−0.60	0.60	0.025±0.013
0532.4−0713	05 32 24.6	−07 13 12.5	K3	−1.45	0.38	0.110±0.032
0532.5−0421	05 32 31.7	−04 21 40.8	K4	−3.50	0.48	0.032±0.014
0532.6−0522	05 32 36.7	−05 22 50.9	K3	−4.00	0.47	0.120±0.024
0533.1−0758	05 33 05.0	−07 58 52.6	K3	−0.30	0.35	0.082±0.028
0533.1+0224	05 33 08.1	+02 24 56.8	K4	−0.20	0.44	0.038±0.015
0533.5−0646	05 33 30.5	−06 46 00.5	G8	−0.35	0.31	0.035±0.015
0534.6+1007	05 34 34.9	+10 07 12.8	K3	−0.25	0.36	0.735±0.056
0534.7−0423	05 34 40.5	−04 23 35.0	K2	−0.31	0.29	0.050±0.015
HBC447‡	05 34 40.7	−05 24 36.2	K3	−1.80	0.35	0.219±0.034
0534.7+1114	05 34 44.3	+11 14 39.2	K4	+0.90	0.32	0.023±0.015
0535.0−0411	05 35 01.3	−04 11 54.4	K1	−0.10	0.41	0.038±0.014
0535.3−0059	05 35 15.2	−00 59 40.0	K3	−2.75	0.39	0.050±0.015
0535.6−0152	05 35 34.1	−01 52 22.8	G9	+2.40	0.32	0.018±0.011
0535.8−0508	05 35 45.0	−05 08 41.2	K6	−2.40	0.48	0.147±0.029
0535.7−0418	05 35 42.0	−04 18 08.7	K3	−0.15	–	0.050±0.015
0536.0−0650†	05 36 00.1	−06 50 09.1	M1	−8.57	–	0.056±0.020
0536.2−0519	05 36 11.8	−05 19 59.0	K4	−24.70	0.45	0.050±0.015
0536.7+0907	05 36 39.6	+09 07 16.4	K1	+0.60	0.54	0.049±0.014
0536.9+0608	05 36 52.8	+06 08 09.3	K0	+1.50	0.44	0.050±0.015
0537.0−0300	05 36 57.6	−03 00 39.0	G2	+1.85	0.25	0.127±0.025
0537.6−0054	05 37 33.7	−00 54 00.9	K4	+0.35	0.31	0.039±0.014
0538.4−0637a	05 38 24.0	−06 37 47.2	K1	−0.15	0.45	0.060±0.018
0538.4−0637b	05 38 24.0	−06 37 47.2	K2	−0.35	0.42	0.060±0.018
0538.6−0856	05 38 34.8	−08 56 39.4	G7	+1.35	0.35	0.242±0.035
0538.8+1302	05 38 45.9	+13 02 57.4	K2	+2.67	0.22	0.032±0.011
0538.9−1321	05 38 51.3	−13 21 21.4	G0	+3.05	0.19	0.031±0.015
0538.9−0249	05 38 54.1	−02 49 00.5	K3	−0.01	0.40	0.063±0.019
0538.9−0624	05 38 56.8	−06 24 35.2	G9	+2.22	0.25	0.101±0.028
0539.2+0101	05 39 14.1	+01 01 01.3	G2	+0.20	0.30	0.076±0.017
0539.3+0918	05 39 20.7	+09 18 26.3	K1	+0.90	0.43	0.044±0.014
0539.4−0346	05 39 26.8	−03 46 54.0	G8	+2.78	0.35	0.060±0.015
0539.6−0242	05 39 36.1	−02 42 03.4	K0	−2.38	0.38	0.071±0.016
0539.8−0205	05 39 45.0	−02 05 00.3	K4	−4.70	0.53	0.052±0.014
0539.8−0138	05 39 48.2	−01 38 39.6	K3	−0.25	0.45	0.038±0.013
0539.9−0443	05 39 53.0	−04 43 25.3	F9	+3.15	0.25	0.052±0.013
0539.9+0915	05 39 55.4	+09 15 38.3	K0	+0.55	0.36	0.058±0.014
0539.9+0956	05 39 56.7	+09 56 40.8	K4	−0.10	0.31	0.377±0.036
0540.1−0627	05 40 05.5	−06 27 49.5	K7-M0	−4.90	–	0.013±0.000
0540.1−0737	05 40 05.8	−07 37 59.0	K3	−2.64	0.25	0.050±0.015
0540.2−0708	05 40 13.8	−07 08 28.6	K0	+0.45	0.35	0.033±0.013
0540.5−0121	05 40 32.6	−01 21 57.0	K5	−0.50	0.40	0.048±0.013
0540.8−0806	05 40 45.9	−08 06 36.1	K5	−0.80	0.58	0.028±0.010
0541.3+0027	05 41 18.5	+00 27 41.2	K2	+0.10	0.46	0.038±0.013
0541.4−0324	05 41 23.8	−03 24 43.3	K1	+0.85	0.45	0.049±0.013
0541.8+0944	05 41 45.1	+09 44 35.5	G6	+2.70	0.22	0.044±0.014
0541.9−0556	05 41 56.1	−05 56 43.7	K5	−2.51	0.56	0.052±0.015
0542.4−0626	05 42 25.9	−06 26 17.6	G7	+1.87	0.30	0.043±0.014
0542.7−0925	05 42 39.6	−09 25 06.1	K1	+1.20	0.38	0.034±0.012
0542.9−0718†	05 42 56.1	−07 18 46.0	M3	−8.90	–	0.115±0.021

misclassifications, since the Hα emission can be strongly variable in some WTTS (Alcalá et al. 1993).

The Hα emission of most of the new PMS stars found in Orion is indeed weak, but with a few exceptions. The Hα emission line in the spectrum of RXJ0513.1+0851 is broad (FWHM $\leq$ 300 km s^{-1}) with W(Hα) = −19.5 ± 0.30 Å . The He I λ5876.7 and λ6678.7 lines are also present in emission (Fig. 3). The He I λ5876.7 line is the 4^3D→3^3P transition, and the He I λ6678.7 line is its singlet 4^1D→3^1P analogue. The ratio of the intensities of these two emission lines in the spectrum of this star is 3:1, which corresponds to the ratio for a dense gas in thermodynamic equilibrium. The star is relatively bright (V≈13.0), its photospheric spectrum is that of a K3 star and its near IR colours ($H-K$=0.15 and $J-H$=0.65) indicate the lack of IR excess (see Fig. 5).

The optical counterparts of RXJ0523.1-0440 and RXJ0536.2-0519 show Hα in emission with W(Hα) = −11.60 ± 0.20 Å and W(Hα) = −24.7 ± 0.25 Å (see Table 3) respectively. Unfortunately, near IR photometry for these two stars is lacking. On the basis only of their Hα emission, these three stars could be classified as CTTS. However, the forbidden lines [SII] $\lambda\lambda$ 4068, 4132, 6717 and 6731 Å and [OI] $\lambda\lambda$ 6300 and 6363 Å are not present in their spectra, suggesting that the emission lines are of chromospheric origin. Thus, we conclude that these stars

Table 3. continued

RXJ	α(2000) h m s	δ(2000) ° ′ ″	Sp.T.	W(Hα) [Å]	W(Li) [Å]	cts/s
(1)	(2)	(3)	(4)	(5)	(6)	(7)
0543.5−0642	05 43 27.4	−06 42 57.0	G9	+1.41	0.19	0.032±0.011
0544.2−0941	05 44 08.3	−09 41 36.9	G9	+2.40	0.30	0.035±0.012
0544.2−1306	05 44 10.3	−13 06 30.8	K1	+0.72	0.25	0.025±0.011
0544.2+0115	05 44 12.4	+01 15 42.6	K3	+0.70	0.32	0.049±0.014
0544.6−0121	05 44 34.0	−01 21 55.9	K4	−1.95	0.41	0.052±0.013
0545.6−1020	05 45 35.0	−10 20 26.3	G7	+1.85	0.20	0.054±0.015
0546.1+1232	05 46 03.4	+12 32 36.2	G9	−0.30	0.30	0.023±0.012
0546.7−1223	05 46 42.5	−12 23 28.8	G5	+2.90	0.20	0.033±0.019
0546.9−0506†	05 46 51.4	−05 06 57.0	K4	−0.20	–	0.027±0.013
0549.6+0232	05 49 37.8	+02 32 59.7	K2	+0.95	0.47	0.030±0.012
0550.6−1249†	05 50 34.6	−12 49 10.0	K6	−1.20	–	0.023±0.013
0551.2+0748†	05 51 09.3	+07 48 57.0	K6	+1.05	–	0.029±0.014
0551.2−0653	05 51 10.8	−06 53 29.7	K1	+1.50	0.43	0.037±0.015
0552.3−0557	05 52 19.8	−05 57 48.9	K2	+1.35	0.33	0.027±0.013
0554.6−0736	05 54 34.1	−07 36 29.3	G6	+2.68	0.22	0.025±0.013
0556.1−0800	05 56 08.0	−08 00 17.5	G8	+2.09	0.30	0.046±0.017
0556.5+0619	05 56 28.1	+06 19 37.3	G9	+2.79	0.19	0.033±0.015
0556.8−0611†	05 56 46.8	−06 11 13.5	K5	−0.15	–	0.038±0.015
0558.0+0929	05 57 57.5	+09 29 03.4	G9	+3.50	0.27	0.025±0.013
0558.0−0145	05 58 02.1	−01 45 29.5	K1	+2.05	0.27	0.036±0.016

† Li I λ 6707 Å absorption to be confirmed because of the low signal-to-noise of the spectrum.
‡ optical counterpart of the source RXJ 0534.7−0524. The X-ray position of the the RASS source is given.

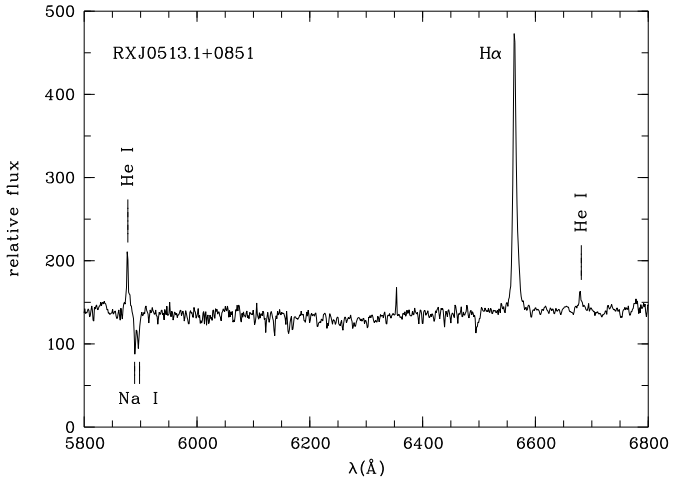

Fig. 3. Spectrum of the optical counterpart of the source RXJ0513.1+0851

are not CTTS, but most probably WTTS with very active chromospheres or WTTS which presented flare activity during the spectroscopic observations. The latter hypothesis is supported by studies of flare activity in WTTS in Orion (Preibish et al. 1995, and references therein) and the recent finding that some of the RASS discovered WTTS in the Chamaeleon SFR show flare activity too (Guenther 1995). A few of these stars, while displaying normally a typical WTTS spectrum, sometimes show a spectrum with characteristics very similar to those of the spectrum in Fig. 3 (Alcalá et al. 1993; Alcalá et al., in preparation).

3.5. *Spatial distribution of the new WTTS*

The spatial distribution of the new WTTS and the known CTTS from the Herbig & Bell catalogue (1988) in the Orion cloud complex is shown in Fig. 4. The outlines of the CO maps by Maddalena et al. (1986) are also overplotted for comparison purposes. While the WTTS are more or less uniformly spread over the whole star forming region, the CTTS are concentrated in the denser parts or cores of the molecular clouds. This confirms previous results found for the Chamaeleon and Taurus-Auriga SFRs (A95; W95).

Most of the CTTS in the Orion complex are located in the Orion nebula, the NGC 2023 and NGC 2024 clusters and in the λ Orionis region. Many WTTS are located also in these areas, but plenty of them are also scattered southwards and northwards of the nebula, where no known CTTS are found and they extend even farther off the limits of the "A" molecular cloud. There are also WTTS located near the NGC 2023 and NGC 2024 clusters and the λ Orionis region, but they are much more scattered than the CTTS. Note that some WTTS are more than 6° distant from the cloud cores. Assuming typical T Tauri ages of $\leq 10^7$, the outermost WTTS should move with mean velocities greater than the typical space velocity given by the velocity dispersion of the CTTS. The existence of low-mass PMS stars rather far from SFRs has been interpreted in terms of "run-away T Tauri stars" (RATTS) by Sterzik et al. (1995), who used 98 of the 112 new WTTS as training sample to preselect potential PMS candidates. The rest of the new WTTS were identified later but independently form the Sterzik et al. (1995) criterion. We investigated the statistical status of these 14 X-ray sources in the

Table 4. Journal of photometric observations

Period	Telescope	Detector	Photometric system	No. of target stars
November 1991	0.8 m	P07029	$UBV(RI)_{\rm KC}$	6
November 1992	2.1 m	InSb	$JHKLM$	45
November 1992	0.8 m	P07029	$UBV(RI)_{\rm KC}$	10
December 1992	1.5 m	P07029	$UBV(RI)_{\rm KC}$	8
January 1994	1.5 m	EMI9789QA	*uvby-β*	20
November 1994	1.5 m	EMI9789QA	*uvby-β*	23
December 1994	0.8 m	P07029	$UBV(RI)_{\rm KC}$	15

context of the pre-selection criterion and found that most of them can be classified as potential T Tauri candidates. We have also checked the status the sources with dubious lithium absorption and obtained similar results. A more complete study of the relation between spatial distribution of the WTTS and their ages will be published in our forthcoming paper.

3.6. *Finding charts of the new WTTS in Orion*

Finding charts for the new WTTS (excluding RXJ 0534.7-0524 which is identified with the star HBC447, see Sects. 3.1 and 3.2) were produced using the Palomar digitised photographic plates and are provided in Fig. 6. In these finding charts North is up, and East is to the left. Each finding chart covers a field of $5'\times5'$ on the sky. The finding charts are sorted by right ascension, and the name of the corresponding X-ray source is also reported for identification in Table 3.

4. The photometric observations

$UBV(RI)_{\rm KC}$, $JHKL$ and *uvby-β* photometric observations for 39, 45 and 42 new WTTS respectively, were carried out at the San Pedro Mártir National Astronomical Observatory (SPMO) in Baja California, México. The data were gathered during several observational runs in the period from November 1991 to December 1994. The basic information on the observing runs, the telescopes and the instrumental set-up used are reported in Table 4.

4.1. $UBV(RI)_{\rm KC}$ *photometry*

The 84 cm telescope and the Lowell I pulse counting photometer of the Sierra San Pedro Mártir National Astronomical Observatory in Baja California, Mexico (SPMO) were used to acquire the $UBV(RI)_{\rm KC}$ photometry of the new Orion WTTS detected with *ROSAT*. The photometer consists of a P07029 photomultiplier in the pulse counting mode cooled to -70°C and a set of Johnson-Kron-Cousins ($UBV(RI)_{\rm KC}$) filters. Details about the instrument can be found in a technical report by Echevarria et al. (1991). A set of 15 reference stars were observed nightly in order to tie the observations to the $UBV(RI)_{\rm KC}$ standard system. The reference stars were selected from the list by

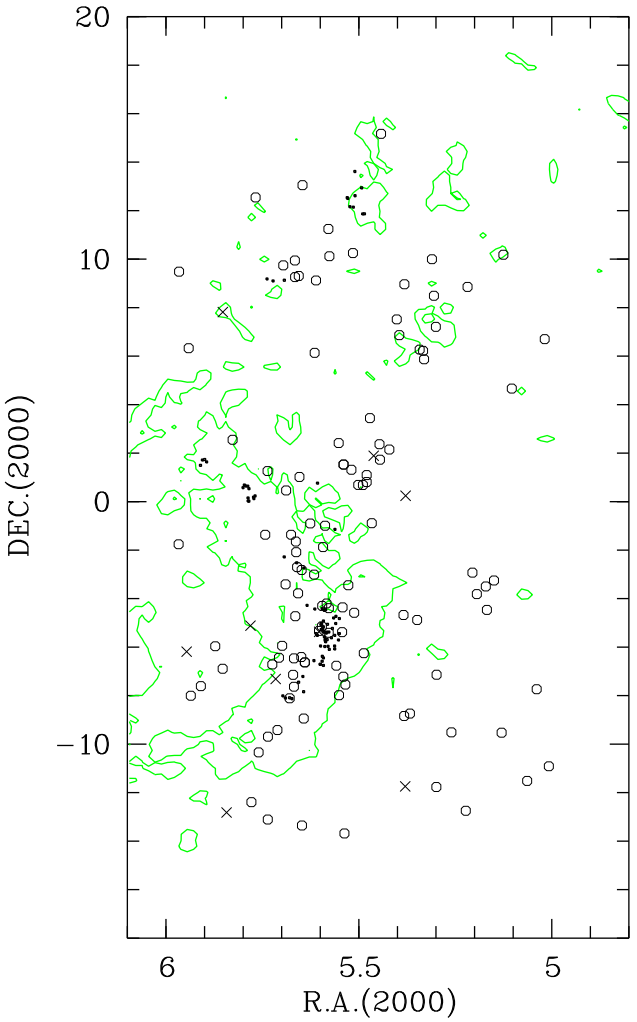

Fig. 4. Spatial distribution of the newly discovered WTTS (○) and of the known CTTS (·) in the Orion SFR. The crosses (×) represent WTTS candidates for which the Li I λ 6707 Å absorption line has to be confirmed. The outlines of the CO line radio-survey by Maddalena et al. (1986) are overplotted as a shaded line. See Sect. 3.5 for further explanations

Landolt (1983) and span from B7 to M0 spectral types. The observations consisted of a of several (10−15 s) integrations on each filter on the star and on the near background. A 20 arcsec diaphragm was used. The data were reduced following the procedures by outlined by Harris et al. (1981). Seasonal mean extinction coefficients given by Schuster (1982) were adopted for the atmospheric extinction correction. The resulting $UBV(RI)_{\rm KC}$ photometry of the program stars is presented in Table 5. The typical observing errors were estimated from the zero point scatter of the standard stars and are the following: σ_U=0.05, σ_B=0.04, σ_V=0.03, $\sigma_{R_{\rm KC}}$=0.02 and $\sigma_{I_{\rm KC}}$=0.02.

4.2. *JHKL photometry*

The SPMO near-IR photometer consists of a InSb diode as detector (cooled at the liquid N_2 temperature) and a $JHKLM$ set of filters. The photometer was attached to the 2.1 m telescope in its infrared configuration ($f/27$) with a chopping secondary mirror (see Roth et al. 1984 for details). A 40 arcsec throw in declination axis and a 10 arcsec diaphragm were used during the observations. In order to fix the observations to the local photometric system, we observed 5 ± 1 near IR standard stars nightly. These stars were taken from the list by Tapia et al.(1986). The data at each night were reduced independently following a standard procedure (e.g. Mitchell 1960). The resulting photometry of the program stars is given in Table 5. Typical errors of the derived magnitudes of the program stars were estimated from integrations in each filter and from the nightly zero point dispersion of the standard stars. The mean errors are: σ_J=0.03, σ_H=0.03, σ_K=0.05 and σ_L=0.30.

The IR colour-colour diagram for the newly discovered WTTS in Orion is shown in Fig. 5 together with the sample of class I and class II IR-sources in the Taurus-Auriga SFR taken from the literature (Herbig & Bell 1988). The normal reddening vector is also shown. Except for three stars (RXJ0534.7-0423, RXJ0535.0-0411 and RXJ0539.8-0205), it can be seen that the WTTS tend to follow the line given by the intrinsic colour line for normal field dwarfs, indicating the lack of (significant) near IR flux-excesses. In the two-colour diagram of Fig. 5, three groups are clearly distinguished: the first group is represented by the IR-sources, the WTTS form the second group and the third group is defined by the field stars. The apparent difference between WTTS and field stars in the IR colour-colour diagram can be ascribed to their different spectral type distributions. While most WTTS have spectral types later than G4, most field stars are earlier than G5.

The spectra of the three discrepant WTTS in the IR colour-colour diagram do not show any untypical characteristic, but we cannot exclude the possible presence of residual circumstellar matter in these stars. For a subsample of 16 WTTS with both $UBV(RI)_{\rm KC}$ and JHK photometric measurements, we derived the spectral energy distributions (SEDs) and confirmed that the new WTTS are "class III" IR sources.

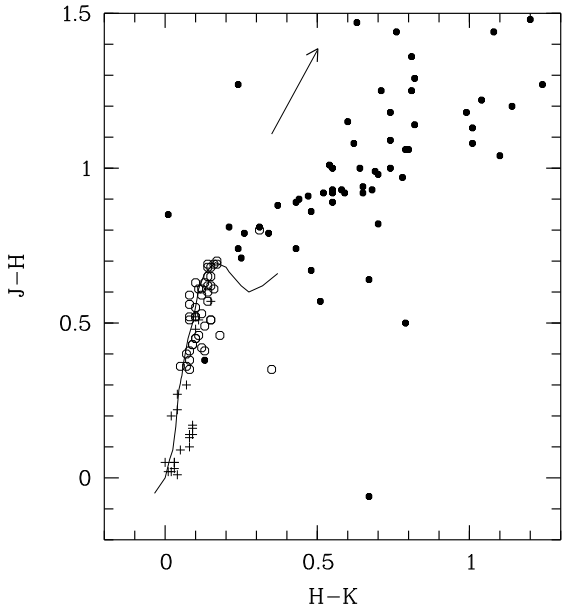

Fig. 5. IR colour-colour diagram for three groups of stars: the new WTTS in Orion (open circles), the class I and class II IR-sources in Taurus-Auriga (filled circles) and normal field stars (crosses). The solid line represents the intrinsic colours for dwarfs from Bessel & Brett (1988) and arrow indicates the normal reddening vector

4.3. *uvby-β photometry*

The SPMO "Danish" grating spectrophotometer for the *uvby-β* photometry is described in detail by Nissen (1984) and by Schuster & Nissen (1988). For a brief description of the photometer consult Terranegra et al. (1994). The photometer consists of six rectangular slots, their corresponding "spectral edge smoothing" filters and sic photomultipliers in a photon counting mode. Four channels are used for simultaneous *uvby* observations and the two remaining channels (the "wide" and "narrow" passbands) are used for the β-index measurements. In both modes, the channels are measured simultaneously but independently from another. Uncooled EMI 9789 QA type photomultipliers are used as detectors in the photon counting mode. The system closely reproduces the *uvby-β* systems of Crawford & Barnes (1970) and of Olsen (1983, 1984). About 15 secondary standard stars were observed from a list kindly provided to us by W. Schuster. Care was taken to include standard stars covering the spectral types and luminosity classes of the program stars. A 20 arcsec diaphragm was used during the observations. The integration time was fixed in order to achieve a photon noise less than 1% for the net signal. All the standard stars were observed at

Table 5. $UBV(RI)_{\rm KC}$ and near IR photometry of the new WTTS in Orion

RXJ	U	B	V	$R_{\rm KC}$	$I_{\rm KC}$	J	H	K	L
0500.4−1054		14.11	13.00	12.31	11.58				
0510.3−0330		12.53	11.74	11.29	10.87				
0513.1+0851						10.20	9.55	9.40	
0515.6−0930		10.46	9.79	9.39	+9.02				
0518.0+0712						10.40	9.89	9.74	
0518.3+0829	12.54	12.04	11.15	10.54	10.11	9.40	8.91	8.78	
0520.0+0612	13.46	12.50	11.31	10.60	10.09	9.17	8.58	8.46	8.62
0520.5+0616	13.88	12.68	11.49	10.80	10.14	9.18	8.61	8.47	8.41
0520.9−0452		9.98	9.53	9.24	8.97				
0522.1−0844	13.59	12.95	12.09	11.60	11.13				
0522.9+0857		11.27	10.28		9.08	8.12	7.52	7.38	7.30
0523.7+0652	14.18	13.87	12.47	11.37	10.83	9.83	9.15	9.00	8.78
0526.7+0143						10.01	9.66	9.58	8.84
0526.8+0222	12.29	12.18	11.51	11.11	10.71	10.05	9.69	9.62	7.42
0528.0−0053						10.74	10.23	10.15	
0528.3+0326	13.09	12.66	11.76	11.18	10.81	9.97	9.45	9.35	8.89
0528.8+0048						11.31	10.90	10.77	
0528.8+0105						10.19	9.51	9.37	8.79
0529.2−0615	12.42	12.12	11.27	10.77	10.31				
0529.4+0041						10.32	9.69	9.59	
0530.1+0041	10.33	10.23	9.54	9.19	8.72	8.15	7.74	7.66	8.00
0530.7−0434	13.90	12.57	11.51	10.79	10.25	9.28	8.60	8.45	7.90
0531.2+0118		13.68	12.84	12.36	11.88				
0532.1−0732						10.55	9.94	9.83	
0532.2−1340		10.21	9.67	9.32	9.07	8.63	8.43	8.45	7.99
0532.4−0713	14.03	13.97	12.86	12.23	11.57	10.70	10.05	9.91	
0532.5−0421	13.80	13.05	11.93	11.27	10.65				
0532.6−0522	14.62	13.19	12.05	11.32	10.37	9.72	9.03	8.87	
0533.1−0758						9.87	9.25	9.10	9.93
0533.5−0646	12.11	11.85	11.12	10.70	10.28				
0534.7−0423	12.55	11.53	11.06	10.73	9.92	10.12	9.86	9.80	
HBC447	13.88	13.61	12.34	11.80	11.25				
0535.0−0411						10.27	9.92	9.57	
0535.3−0059		15.10	14.06	13.22	12.61				
0535.8−0508	15.61	14.41	12.91	12.09	11.31				
0536.7+0907						10.43	9.82	9.70	
0536.9+0608						10.81	10.36	10.26	
0537.0−0300	11.11	10.97	10.25	9.79	9.37	8.91	8.48	8.39	8.59
0537.6−0054						9.67	9.04	8.91	
0538.6−0856						8.50	8.04	7.93	7.69
0538.9−1321		11.20	10.63	10.29	9.96				
0538.9−0249						10.93	10.32	10.16	
0538.9−0624						9.63	9.23	9.16	8.55
0539.2+0101						9.73	9.20	9.08	8.68
0539.4−0346						9.78	9.33	9.23	
0539.6−0242	11.21	10.92	10.06	9.51	9.11	8.53	8.01	7.91	7.78
0539.8−0205						10.75	9.95	9.64	
0539.9−0443						9.61	9.25	9.20	10.00
0540.1−0737						9.66	9.20	9.02	
0540.2−0708						10.81	10.29	10.21	
0540.8−0806		14.23	12.87	12.10	11.29				
0541.3+0027						10.95	10.26	10.09	
0541.4−0324	12.63	12.70	11.75	11.18	10.66	10.07	9.51	9.43	
0541.8+0944	10.88	10.73	10.07	9.67	9.28				
0541.9−0556						10.74	10.02	9.96	
0542.4−0626						10.52	10.14	10.06	9.80
0542.7−0925						10.51	9.96	9.86	
0543.5−0642						10.62	10.19	10.10	9.42
0544.2−0941	13.21	12.93	12.22	11.77	11.35				
0544.2−1306						9.11	8.49	8.35	7.76
0544.2+0115						10.01	9.42	9.34	
0545.6−1020	12.33	12.10	11.43	11.01	10.61				
0549.6+0232	13.86	13.24	12.33	11.75	11.20				
0551.2−0653	12.51	12.08	11.24	10.73	10.26				
0554.6−0736	12.43	12.33	11.71	11.31	10.93				
0556.1−0800	13.11	12.78	12.04	11.59	11.19				
0556.5+0619	11.53	11.19	10.41	9.96	9.52				
0558.0−0145	13.55	12.93	12.08	11.55	11.08				

least twice during the run. The instrumental magnitudes and colors were transformed to the standard system following usual procedures (cf. Terranegra et al. 1994). The NABAPHOT utility package of the San Pedro Mártir Observatory was used to reduce the data (Arellano-Ferro & Parrao 1988). The resulting *uvby-β* photometry of the program stars observed is listed in Table 6. In this table we give the quantities c_1, m_1 (cf. Strömgren 1966) and the β index (Crawford 1979). The typical mean errors of these measured quantities are σ_y=0.20, σ_{b-y}=0.05, σ_{c_1}=0.08, σ_{m_1}=0.05 and $\sigma_{H\beta}$=0.06.

Table 6. *uvby*$-\beta$ photometry

RXJ	V	$b-y$	m_1	c_1	$H\beta$
0500.4−1054	13.03	0.67	0.43	0.27	$2.46^{e,v?}$
0501.1+0642	12.62	0.64	0.44	–	2.55
0502.4−0744	11.21	0.46	0.20	0.38	2.58
0506.2+0439	13.58	1.15	–	0.30	2.37^{e}
0507.5+1010	10.45	0.47	0.24	0.27	2.60
0509.0−0315	11.27	0.48	0.21	0.32	2.57
0510.1−0427	11.58	0.61	0.51	0.12	2.53
0510.3−0330	11.38	0.52	0.22	0.32	2.57
0511.7−0348	11.93	0.51	0.33	0.23	2.59
0512.3−0255	10.47	0.46	–	0.20	2.43^{e}
0513.1+0851	13.08	0.80	0.37	0.26	2.60
0513.4−1244	10.77	0.38	0.21	0.34	2.61
0515.6−0930	9.84	0.42	0.27	0.28	2.59
0517.9−0708	10.70	0.52	0.35	0.27	2.56
0518.0−1146	11.51	0.55	0.36	0.25	2.58
0518.0+0712	13.08	0.63	0.32	0.36	2.63
0518.3+0829	11.68	0.54	0.25	0.35	2.58
0520.0+0612	11.56	0.70	0.47	0.27	2.55
0520.5+0616	12.20	0.69	0.43	0.28	2.56
0520.9−0452	9.48	0.31	0.16	0.40	2.64
0522.9+0857	11.13	0.61	0.21	0.36	2.59
0523.7+0652	12.79	0.84	0.45	0.23	2.60
0526.7+0143	12.82	0.62	0.25	0.50	$2.45^{e,v?}$
0526.8+0222	11.75	0.46	0.18	0.43	2.62
0528.3+0326	12.04	0.59	0.27	0.37	2.60
0528.8+0048	14.04	0.59	0.23	0.33	2.62
0529.2−0615	11.19	0.53	0.26	0.27	2.54
0529.4+0041	12.56	0.64	0.41	0.28	2.55
0530.1+0041	9.53	0.44	0.19	0.39	2.63
0530.7−0434	11.57	0.72	0.41	0.27	2.59
0532.1−0732	12.57	0.64	0.37	0.34	2.55
0532.2−1340	9.61	0.35	0.17	0.41	2.54
0532.4−0713	12.82	0.67	0.32	0.33	2.62
0532.5−0421	11.89	0.63	0.46	0.24	2.58
0532.6−0522	12.19	0.73	0.43	0.26	2.57
0533.1−0758	11.76	0.71	0.43	0.35	2.56
0534.7−0423	13.22	0.68	0.43	0.32	2.66
0535.0−0411	12.02	0.58	0.28	0.33	2.49^{e}
0535.3−0059	12.79	0.73	0.38	0.44	2.69
0537.0−0300	10.14	0.47	0.17	0.46	2.60
0538.6−0856	9.92	0.48	0.25	0.35	2.59
0541.8+0944	10.09	0.42	0.20	0.35	2.51

e: $H\beta$ in emission; $v?$: possibly variable Hβ.

5. Conclusions

X-ray data from the RASS in an area of about 450 square degrees in direction to the Orion cloud complex were obtained. The mean spatially projected density of X-ray sources in this region is a factor of about two higher than that for the RASS elsewhere 5.6% of the RASS sources in this region are identified with previously known pre-main sequence stars. X-ray light curves were obtained for more than 200 sources detected with a high S/N ratio. Only three sources were found to show significant variability in X-rays, but we cannot exclude the possibility of low-level X-ray variability, observable as scan-to-scan variations, in the rest of the sources.

181 (spatially unbiased) RASS sources, widely distributed over the entire cloud complex, were investigated spectroscopically. 62% of them could be identified with WTTS. The new WTTS are found to be widely distributed throughout the entire Orion star forming region, while the CTTS in this region tend to be concentrated mainly in the cloud cores.

A sample of 39 WTTS was observed in the $UBV(RI)_{\rm KC}$ photometric system. Near-IR $JHKL$ photometry for 45 WTTS was also obtained. In addition, *uvby-β* photometric measurements were obtained for a sample of 42 WTTS. The spectral energy distributions of these WTTS and their position in the IR colour-colour diagram, confirms that they are "class III" IR sources.

Acknowledgements. We are very grateful to Prof. I. Appenzeller, E. Covino , M. Sterzik and R. Neuhäuser for valuable comments and suggestions for this research work. The *ROSAT* team, and in particular the EXSAS group at MPE are also acknowledged for assistance and help with the *ROSAT* data reduction. G. García of the SPMO efficiently assisted us with the near IR observations at the telescope and W. Schuster and L. Parrao helped us to configurate a subset of standard stars and instructing us with the reductions of the *uvby*-beta observations, respectively The *ROSAT* project has been supported by the Bundesministerium für Bildung, Wissenschaft, Forschung und Technologie and the Max-Planck-Gesellschaft. This research has made use of the SIMBAD database, operated at CDS, Strasbourg, France.

References

Alcalá J.M., Covino E., Franchini M., et al., 1993, A&A 272, 225

Alcalá J.M., Krautter J., Schmitt J.H.M.M., et al., 1995, A&AS 114, 109 (A95)

Arellano-Ferro A., Parrao L., 1988, Techn. Report No. 57, Instituto de Astronomia, UNAM, Ap. Postal 70-264, Mexico 04510, D.F.

Blaauw A., 1991, in "The physics of star formation and early stellar evolution". In: Lada C.J., Kylafis N.D. (eds.), Vol. 342 of NATO ASI Series C. Dordrech: Kluwer

Bodenheimer P., 1965, ApJ 142, 459

Brand J., Wouterloot J.G.A., 1991, in "Low mass star formation in southern molecular clouds". In: Bo Reipurth (ed.), ESO Scientific Report No. 11, p. 1

Crawford D.L., 1979, in "Problems of Calibrations of Multicolor Photometric Systems". In: Philip A.E. (ed.), Dudley Obs. Rep. No. 14

Crawford D.L., Barnes J.V., 1970, AJ 75, 978

Duerr R, Imhoff C.L., Lada C.J., 1982, ApJ 261, 135

Echevarría J., Murillo J., Hiriart D., 1991, Manual de Usuario del Fotómetro Cuenta PulsosII, Observatorio Astronómico

Nacional, Apartado postal 877, Ensenada 22800, B.C. México
Feigelson E.D., 1987 in Protostars and molecular clouds. In: Montmerle Th. and Bertout C. (eds.), CEN Saclay, Gif-sur-Yvette, p. 123
Gagné M., Caillault J-P., 1994, ApJ 437, 361
Genzel R., Stutzki J., 1989, ARA&A 27, 41
Giacconi R., Gursky H., 1974, "X-ray Astronomy". Dordrecht: Reidel
Guenther E., 1995, in Proceedings of the ESO workshop "The role of dust in the formation of stars". In: Ralf Siebenmorgen and Hans Ulrich Käufl. (eds.)
Harris W.E., Fitzgerald M.P., Reed B.C., 1981, PASP 93, 507
Herbig G.H., Bell K.R., 1988, Lick Observatory Bulletin, No. 1111
Kogure T., et al., 1989, PASJ 41, 1195
Krautter J., Alcalá J.M., Wichmann R., Neuhäuser R., Schmitt J.H.M.M., 1994, Rev. Mex. Astron. Astrofis. 29, 41
Ku W.H.-M., Chanan G.A., 1979, ApJ 228, L33
Landolt A.U., 1983, AJ 88, 439
Maddalena R.J., Morris M, Moscowitz J., Thaddeuss P., 1986, ApJ 303, 375
Mitchell R., 1960, ApJ 132, 68
Neuhäuser R., Sterzik M.F., Schmitt J.H.M.M., Wichmann R., Krautter J., 1995, A&A 297, 391
Nissen P., 1984 Technical Report of the SPMO, Instituto de Astronomía, P.O. Box 439027, San Diego, CA 92143-9027, U.S.A.
Olsen E.H., 1983, A&AS 54, 55
Olsen E.H., 1984, A&AS 57, 443
Pfeffermann E., et al., 1986, Proc. SPIE 733, 519
Preibish Th., Neuhäuser R., Alcalá J.M., 1995, A&A 304, L13
Roth M, Iriarte A., Tapia M., Reséndiz G., 1984, Rev. Mex. Astron. Astrofis. 9, 25
Schuster W.J., 1982, Rev. Mex. Astron. Astrof. 5, 149
Schuster W., Nissen P., 1988, A&AS 73, 225
Sterzik M., Alcalá J.M., Neuhäuser R., Schmitt J.H.M.M., 1995, A&A 297, 418
Strömgren B., 1966, ARA&A 4, 433
Tapia M., Neri L., Roth M., 1986, Rev. Mex. Astron. Astrofis. 13, 115
Terranegra L., Chavarría-K. C., Díaz S., González-Patiño D., 1994, A&AS 104, 557
Trümper J., et al., 1991, Nat 349, 579
Voges W., 1992a, Satellite Symp. No. 3 ESA ISY-3, p. 155
Voges W., 1992b, The ROSAT all-sky survey and the first identifications of X-ray sources using digitised optical plates. In: MacGillivray H.T., Thomson E.B. (eds.), Digitised optical sky surveys. Kluwer, p. 452-463
Walter F.M., Brown A., Mathieu R.D., Myers P.C., Vrba F.J., 1988, AJ 96, 297
Wichmann R., et al., 1995, A&A (submitted) (W95)
Wiramihardja S.D., et al., 1989, PASJ 41, 155
Zimmermann, et al., 1994, EXSAS user's Guide MPE Report No. 257

Fig. 6. Finding charts for the new WTTS. In these finding charts North is up, and East is to the left. Each finding chart covers a field of $5' \times 5'$ on the sky. The finding charts are sorted by right ascension, and the name of the corresponding X-ray source is at the top of each field for identification in Table 3

Fig. 6. continued

Fig. 6. continued

Fig. 6. continued